Primljen / Received: 9.5.2018.
Ispravljen / Corrected: 7.9.2020.
Prihvaćen / Accepted: 26.11.2021.
Dostupno online / Available online: 10.1.2022.

Energy based three-dimensional damage index for monitoring and damage detection of concrete structures

Authors:

[1]**Nikola Stojić**, MCE
n_stojic@yahoo.com

[2]Prof. **Tamara Nestorović**, PhD. CE
tamara.nestorovic@rub.de

[3]Prof. **Dragoslav Stojić**, PhD. CE
dragoslav.stojic@gmail.com

[2,3]**Nemanja Marković**, PhD. CE
nemanja.markovic@gaf.ni.ac.rs
Corresponding author

[4]**Nenad Stojković**, PhD. CE
svnenad@yahoo.com

[5]**Nikola Velimirović**, PhD. CE
nvelimirovic@np.ac.rs

[1]University of Niš, Serbia
[2]Ruhr University in Bochum, Germany
Faculty of Civil Engineering and Ecology engineering
[3]University of Niš, Serbia
Faculty of Civil Engineering and Architecture
[4]University of Niš, Serbia
The Academy of Applied Technical and Preschool Studies
[5]State University of Novi Pazar, Serbia
Department of Technical sciences

Research Paper

Nikola Stojić, Tamara Nestorović, Dragoslav Stojić, Nemanja Marković, Nenad Stojković, Nikola Velimirović

Energy based three-dimensional damage index for monitoring and damage detection of concrete structures

A novel approach to active structural health monitoring and damage detection of massive reinforced concrete structures using piezoelectric smart aggregates is presented in this paper. An innovative three-dimensional damage index, based on wavelet signal decomposition and energy of wave propagation, is derived in matrix form. Although the proposed three-dimensional damage index can be used for all types of reinforced concrete structures, it is primarily recommended for massive infrastructure buildings. The approach proposed in this paper is theoretically considered for an arbitrary shape of a reinforced concrete element, and it is numerically verified for various scenarios by varying the geometry of reinforced concrete elements, as well as the position, size and quantity of damage. Quasi-static analysis of piezoelectric smart aggregates is modelled using a standard finite element method, and the explicit finite element method is successfully applied in this research for modelling propagation of ultrasonic waves. The results based on numerically generated simulations indicate that the new approach to non-destructive damage detection using three-dimensional damage indexes is quite promising.

Key words:

damage detection, nondestructive evaluation, structural health monitoring, numerical simulation, damage indices

Prethodno priopćenje

Nikola Stojić, Tamara Nestorović, Dragoslav Stojić, Nemanja Marković, Nenad Stojković, Nikola Velimirović

Energetski baziran trodimenzionalni indeks oštećenja za praćenje i otkrivanje oštećenja na betonskim građevinama

U radu je prikazan novi pristup koji omogućuje aktivno praćenje stanja konstrukcija i otkrivanje oštećenja na masivnim armiranobetonskim konstrukcijama, a utemeljen je na primjeni piezoelektričnih pametnih agregata. U matričnom je obliku izveden inovativni trodimenzionalni indeks oštećenja baziran na valićnoj dekompoziciji signala i energiji prostiranja valova. Iako se predloženi trodimenzionalni indeks oštećenja može koristiti za sve vrste armiranobetonskih konstrukcija, prije svega se ipak preporučuje za masivne infrastrukturne građevine. Pristup predložen u ovom radu teoretski je izveden za proizvoljni oblik armiranobetonskog elementa, te je numerički provjeren u raznim scenarijima variranjem geometrije armiranobetonskih elemenata, isto kao i položaja, veličine i rasprostranjenosti oštećenja. Kvazistatička analiza piezoelektričnih pametnih agregata modelirana je pomoću standardne metode konačnih elemenata, a u ovom je istraživanju uspješno primijenjena eksplicitna metoda konačnih elemenata za modeliranje prostiranja ultrazvučnih valova. Rezultati bazirani na numerički generiranim simulacijama upućuju na perspektivnost novog pristupa za nerazorno otkrivanje oštećenja pomoću trodimenzionalnih indeksa oštećenja.

Ključne riječi:
otkrivanje oštećenja, nerazorno ocjenjivanje, praćenje stanja konstrukcija, numerička simulacija, indeksi oštećenja

1. Introduction

Reinforced concrete (RC) structures are mainly used for the construction of civil engineering buildings of national importance, such as long span bridges, dams, and skyscrapers. Due to an extremely big size of these buildings, all the elements that are significant from the structural capacity and safety point of view, can be considered in the context of damage detection as massive three-dimensional elements. During the service life of RC structures, a number of important problems need to be tackled in order to preserve an adequate level of safety and reliability of buildings. Various influences affecting structures, such as hazardous events (earthquakes, hurricanes, and tsunamis), vehicle collisions on bridges, and high cycle fatigue loads, can cause significant damage to structural elements and increase the risk of structural collapse. It is necessary to protect RC structures by systems that can detect the occurrence of damage and its propagation over short time, especially for infrastructure facilities, the aim being to provide enough data for decision makers. Timely reactions can save people's lives, while also lowering cost of maintenance and rehabilitation of buildings. In turn, this would decrease losses appearing while the building is not used, increase the safety of structures, and lower the risk of building collapse.

Piezoelectric smart aggregates (PZT SA), as multifunctional devices, are inter alia used for detecting damage to reinforced concrete structures. The use of PZT SA enables damage detection in RC girder elements [1, 2]. Nondestructive detection of damage induced by cyclic loading of RC columns and columns strengthened by fibre-reinforced-polymeric (FRP) strips, based on the use of PZT SA, is reported in [3, 4]. The PZT SA embedded in a framed RC structure were applied as active devices for detecting damage and monitoring further damage propagation caused by experimental simulation of earthquake load [5,6]. The mentioned experimental research points to a very good potential of using PZT SA for active structural health monitoring (SHM) of RC structures. Two main principles of damage detection are used in literature:

- detection based on wave propagation energy
- detection based on impedance.

The first concept, which presents the use of "Pitch-Catch" configuration of the actuators and sensors, will be applied in this paper. It means that one PZT SA is used as the actuator for inducing mechanical wave propagation through RC structure, while the other PZT SA is used as the sensor for detecting the incoming wave.

If a direct relation can be established between certain characteristics gained from sensor output signals and structural damage, then such a relation can be regarded as the damage index (DI). Damage indices based on wave propagation and analysis of output signals can be divided into three categories:

- damage index in time domain
- damage index in frequency domain,
- damage index in time-frequency domain.

Depending on the type of elements that are considered, damage indices can be divided into linear (one-dimensional), surface (two-dimensional) and space (three-dimensional) damage indices. The space (3D) damage index in time domain will be presented in this paper. Many different damage indices in time domain have so far been used, such as the peak-to-peak amplitude DI [7], root-mean-square DI [8] and root-mean-square-deviation (RMSD) DI [9, 10]. Various variations of indices have been successfully applied on the basis of the sensor's output signal energy [11-13], combination of amplitude and time of flight (ToF) [14], and attenuation-based DI [15]. More complex damage indices are time-reversal damage indices [16], damage indices based on nonlinear time series analysis [17], and Pearson correlation coefficient damage indices [18]. The sensor history damage index in matrix form was used for monitoring damage propagation in RC bridge girders over time [19]. The damage index in frequency domain is presented in [19, 20], while the DI based on energy of the first intrinsic mode function (IMF) obtained by Hilbert transformation of signal is used in [21]. All the above-mentioned damage indices, either in time or frequency domain, are one-dimensional damage indices.

Multidimensional DI is far less used in relevant literature for damage detection of structures. Above all, two-dimensional damage index, based on the wavelet signal decomposition and energy of output signal, has been used for monitoring damage propagation in RC shear walls [22]. Three-dimensional DI, based on the use of the modified matrix subtraction method (MMSM), as well as tensor method (TM) DI, have been used for determining damage to RC columns of a railway bridge [23]. Also, 3D DI has been presented based on vibration characteristics of a frame RC structure [24]. Similarly, the Levenberg-Marquardt local search with generic algorithm for damage reconstruction has been used for the same type of structures [25]. The presented 3D DI analyses the structure globally and its elements are considered as linear, which is reasonable for RC frame structures. However, if massive infrastructure facilities or other large-scale RC structures are considered, then it is necessary to treat the structure from "the inside", that is, each element must be observed as a three-dimensional element, and the damage level must be monitored inside each element. The obtained results of damage detection within a massive RC element can further be used for global analysis of structural capacity and safety.

The already introduced damage indices provide information in one or two dimensions, which is adequate for the analysis of linear or surface elements. Current three-dimensional damage indices are related to the global analysis of structures,

and are used for damage detection of frame structures. According to the best knowledge of the authors and detailed research of relevant literature, no damage index that can give information about damage inside massive RC elements has so far been developed. The aim of this paper is to present 3D DI that will be capable of detecting damage and partly determining the position of damage inside individual elements of RC structures. We consider that the existing damage indices do not satisfy practical needs for SHM of massive RC structures, infrastructural buildings in particular. That is why it is necessary to work on further development of 3D damage indices and methods for damage localization in space.

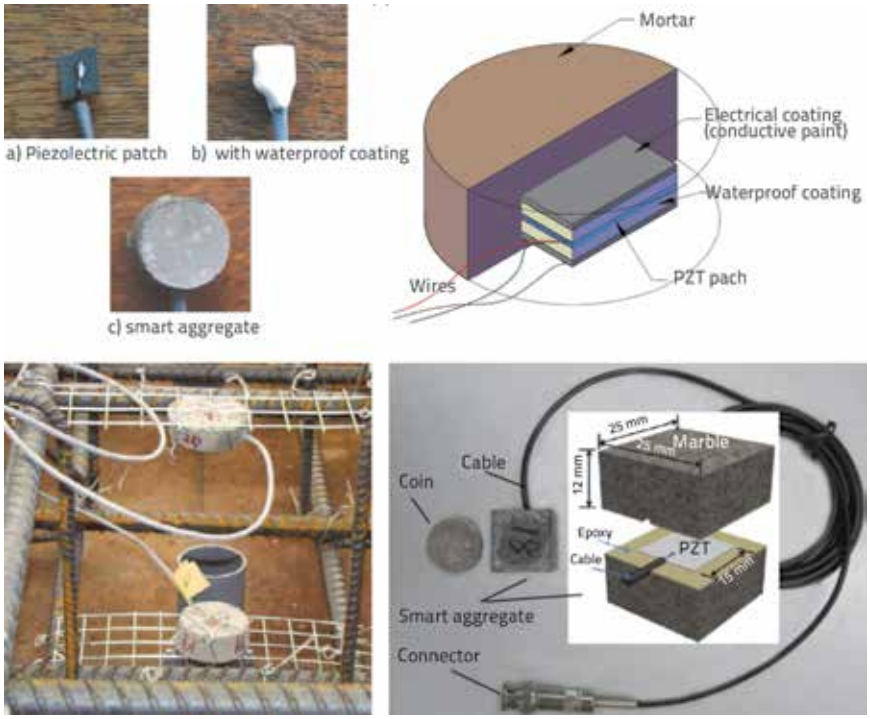

Figure 1. Piezoelectric smart aggregate (SA): Top-left: SA transducers manufactured at ULB-BATir, Top-right: Illustration of a SA [27], Bottom-left: SA embedded in concrete specimen [28], Bottom-right: Structure of SA [29]

2. Piezoelectric smart aggregates and damage detection approach

Piezoelectricity describes the phenomenon of generating an electric field when a material is subjected to mechanical stress (direct piezoelectric effect) or, conversely, generating a mechanical strain in response to an applied electric field (inverse piezoelectric effect). For linear piezoelectric materials, a constitutive relation is established between mechanical and electrical variables [26]:

$$\{S\} = [s]\{T\} + [d]^t \{E\} + \{\alpha\}\theta \quad (1)$$

$$\{E\} = [g]\{T\} + [B]\{D\} + \{\tilde{E}\}\theta \quad (2)$$

where:

{S}, {T} - strain and stress vectors
{E}, {D} - electric field and electric displacement vectors
θ - temperature
{α}, {$\tilde{E}$} - coefficient of thermal expansion and electric displacement temperature coefficient
[d]t, [g] - matrix of coupling coefficients and matrix of piezoelectric voltage coefficient
[β] - matrix of dielectric constants
[s] - compliance matrix.

Equation (1) is an actuation equation that can predict how much electric field is generated by a given mechanical stress. Conversely, Equation (2) is a sensor equation that can predict how much mechanical strain is generated by a given mechanical stress.

Piezoelectric patches are very brittle and sensitive to moisture and were, therefore, not used for damage detection in RC structures. Nevertheless, these disadvantages were eliminated after development of PZT SA, Figure 1. PZT SA are made in such a way that the PZT patch is first protected by a waterproofing layer, connected to electric wires, and is placed in a small formwork into which fresh concrete is poured. After hardening of concrete, PZT SA is ready for embedding in a RC structural element, Figure 1, bottom left, Figure 2, left. By forming this small smart concrete block, the brittle PZT patch is protected from mechanical impacts, vibrations or moisture, which appear in real large-scale structures. Smart aggregates are embedded in RC elements by fixing them to the reinforcement or formwork. It should be noted that SA must keep the required position and orientation so that mechanical waves can be oriented towards the preferred direction. PZT SA have good qualities such as: simple production and use, low price, fast response, large frequency range, high reliability, multifunctionality, resistance to chemically aggressive substances, and resistance to UV rays. There are some disadvantages too: low output voltage (it is necessary to use a voltage amplifier), high resistance, moisture sensitivity, and sensitivity to mechanical impacts of PZT patch (which is neutralized by creating SA), as well as big number of SA that are needed for SHM of RC structures.

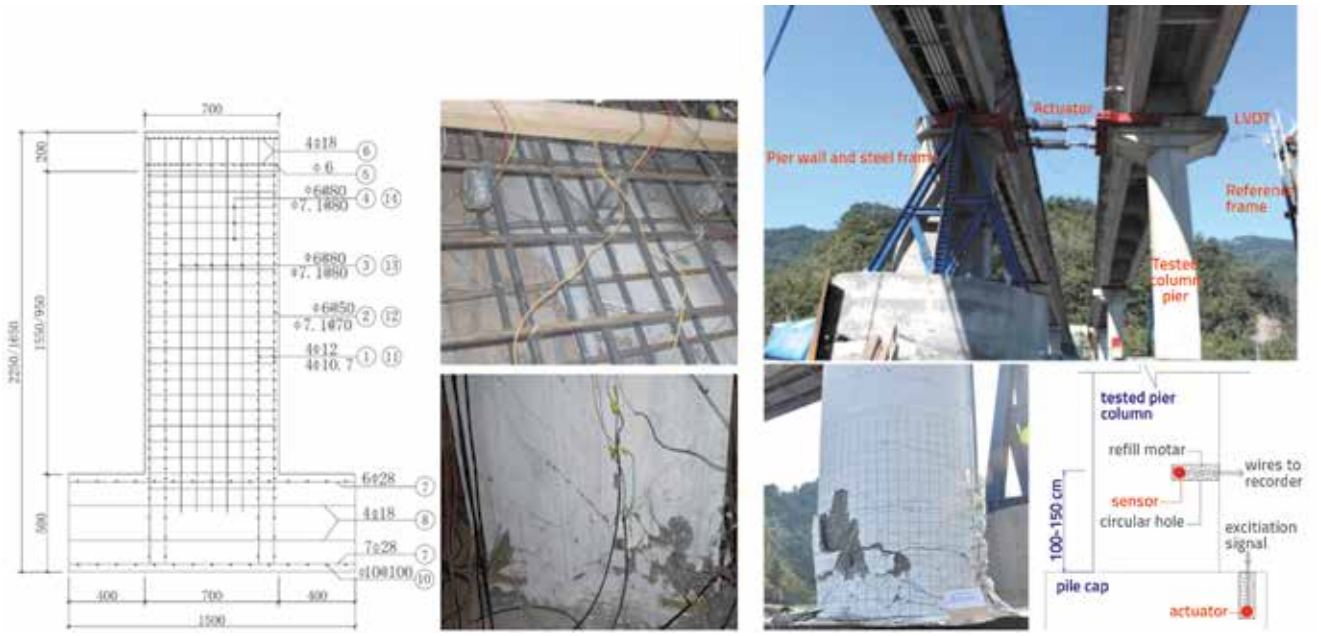

Figure 2. Implementation of smart aggregate for damage detection: Monitoring of reinforced concrete shear walls [30] (left); Monitoring of Niu-Dou Bridge, Taiwan (right) [28]

The general concept of damage detection in RC structures by PZT SA is based on employing piezoelectric effects. The inverse piezo effect is used to induce elastic propagation of mechanical waves, while the direct piezo effect is used to detect the incoming mechanical wave. Actuating the PZT SA actuators is mostly done by electric voltage in short time signals (Hanning windowed tone burst, Rick's signals) or by continuously longer time signals (sweep sine signals). The energy method is based on the fact that the energy of transmitted waves weakens with the development of damage, which directly influences the output signal of sensors. Monitoring the change of energy of the output sensor signal is done by wavelet decomposition. With this approach, it is possible to detect the occurrence of damage and its further propagation in time. Figure 2 shows some examples of implementation of the energy approach, by using the linear damage index (equation 10) for damage detection of RC wall and monitoring of further propagation of damage in a concrete bridge pier.

3. Energy based one-dimensional rmsd damage index

The root-mean-square deviation (RMSD) damage index based on wavelet signal decomposition and wave energy is frequently used for detecting damage to linear RC elements (beams, columns and trusses). In this paper, this DI will be used as one input parameter for the derivation of 3D DI.

3.1. Wavelet signal decomposition

The wavelet signal decomposition is used in this paper as the signal processing tool to analyse the sensor output signal of the embedded PZT SA. The wavelet analysis involves splitting of the signal into the shifted and scaled versions of the original (mother) wavelet. In the wavelet signal decomposition, the signal is split into two signals called *approximation* and *detail*. The approximation is then split in a new approximation and detail, and the procedure is further repeated. The detail can also be divided into new approximations and details, but this was not done in this study because the details have a marginal energy, and they are not of considerable importance for this analysis. A wavelet is a waveform of effectively limited duration that has an average value of zero:

$$\int_{-\infty}^{+\infty} \Psi_{(t)} dt = 0 \tag{3}$$

Using a selected mother wavelet function $\psi(t)$ (in this paper, Daubechies wavelet base db9 is used as the mother wavelet), the continuous wavelet transform (CWT) of a function $f_{(t)}$ is defined as:

$$W_f(a,b) = \frac{1}{\sqrt{a}} \int_{-\infty}^{+\infty} f_{(t)} \overline{\Psi}\left(\frac{t-b}{a}\right) dt \tag{4}$$

where $a > 0$ and $b \in R$ are the dilation and translation parameters, respectively. The bar over $\psi_{(t)}$ indicates its complex conjugate. Wavelet decomposition has been used in this paper because of its

excellent properties and possibilities for the application in relatively narrow frequency bands and a relatively short time window.

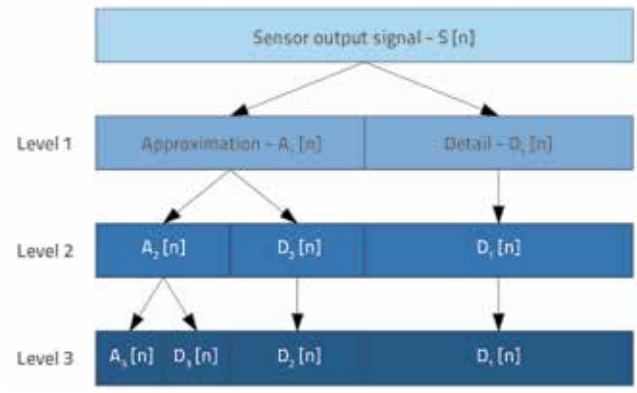

Figure 3. Algorithm of continuous wavelet transform of sensor output signal

Energy based one-dimensional damage index

The output signal *S* in time domain measured using the PZT SA sensor is first decomposed, using the *n*-level wavelet packet decomposition, into 2^n signal sets:

$$\left\{X_1,\ X_2,\ldots,\ X_j,\ldots,X_{2^n-1},X_{2^n}\right\} \tag{5}$$

$$X_j=\left[x_{j,1},x_{j,2},\ldots,x_{j,m}\right] \tag{6}$$

where *m* is the number of sampling data. The energy of the decomposed output signal detected in PZT SA can be defined using the following relation:

$$E_{i,j}=\left\|X_j\right\|_2^2=x_{j,1}^2+x_{j,2}^2+\ldots+x_{j,m-1}^2+x_{j,m}^2 \tag{7}$$

where *i* is the time index and *j* is the level of wavelet decomposition ($j = 1,\ldots, 2^n$). The energy vector for damage state at time index *i* is defined as:

$$E_i=\left[E_{i,1},E_{i,2},\ldots,E_{1,2^n}\right] \tag{8}$$

For the healthy state of the structure, the energy vector is defined as:

$$E_h=\left[E_{h,1},E_{h,2},\ldots,E_{h,2^n}\right] \tag{9}$$

One-dimensional root-mean-square deviation (RMSD) damage index based on the wave energy and wavelet signal decomposition at time *i* is defined as:

$$DI=\sqrt{\frac{\sum_{j=1}^{2^n}(E_{i,j}-E_{h,j})^2}{\sum_{j=1}^{2^n}(E_{h,j})^2}} \tag{10}$$

An increase of the damage index is associated with an increase of damage within a structure, giving the possibility to track structural state using the damage index defined in the presented way. This DI provides information about the occurrence of damage near the actuator-sensor direction. Consequently, it is suitable for monitoring linear RC elements.

4. Novel energy based three-dimensional damage index

A new three-dimensional damage index for active SHM of massive RC structures will be introduced in this paper. Firstly, the damage index will be derived for the general form, and then its verification will be shown on the chosen models.

An arbitrarily chosen three-dimensional RC body is considered with respect to a 3D Cartesian local coordinate system (LCS) (x, y, z). With respect to the LCS, the body is discretized by mutually perpendicular planes $F_{xy}^k, F_{xz}^j, F_{yz}^i$ (i = 1, 2, ..., p; 1 = 1, 2, ..., q; k = 1, ,2, ..., r) as shown in *Figure 4*. The planes $\Delta_{z1},\Delta_{z2},\ldots,\Delta_{zk},\ldots,\Delta zr-1$, are set at mutual intervals , which are different in general case. The other two types of orthogonal planes are also set at mutual intervals which can differ in length.

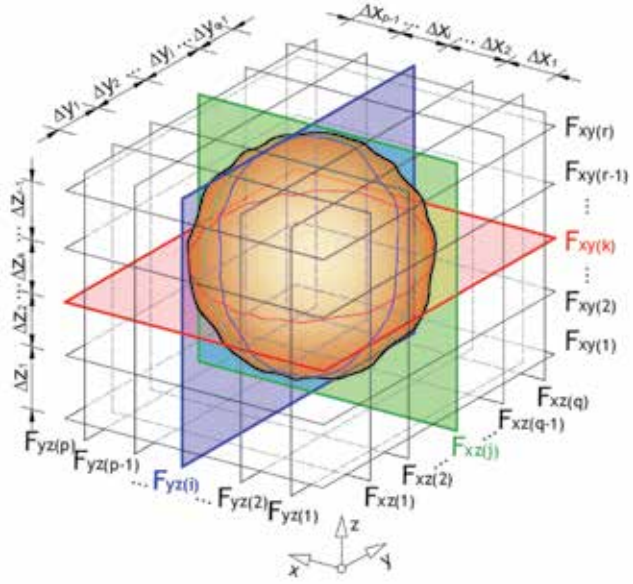

Figure 4. Discretization of arbitrary reinforced concrete body using orthogonal planes

Figure 5 shows three mutually orthogonal planes which form three intersect directions d_{xjk}, d_{yik}, d_{zij}. PZT SA are set at the intersection of the directions with the monitoring body of random shape (PZT smart aggregates SA_{xjk} and SA'_{xjk} are set at the intersection with the body). Point T_{ijk} is the intersection point of three directions shown in Figure 5, and it represents the sub-domain B_{ijk}. The sub-domain B_{ijk} is formed by the intersection of imagined mutual planes (Figure 5 right), which are placed in the middle of the interval between the planes, and other two orthogonal directions $F_{yz}^{k-1}, F_{yz}^k, F_{yz}^{k+1}$ i $F_{yz}^{j-1}, F_{yz}^j, F_{yz}^{j+1}$. Each point of intersection which stands for one sub-domain of the whole concrete body will have the unique value in the 3D damage index.

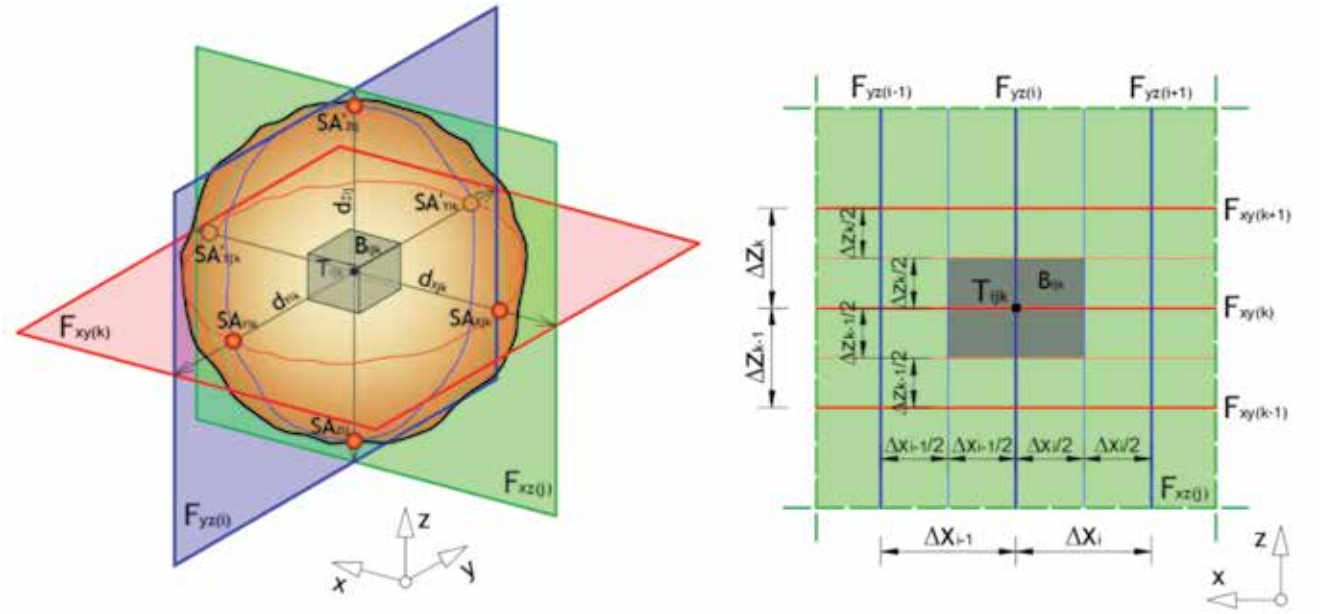

Figure 5. Creating intersection directions and points that represent sub-bodies

At the intersection of all xz and xy planes, we get d_{xjk} (j = 1, 2, ..., q; k = 1, 2, ..., r) directions, as shown in Figure 6. The orthogonal projection (thicker purple line) is formed on the imagined plane yz outside the body by sectioning using section plane 1-1 through the body. The projection of all directions (points P_{xjk} and P'_{xjk}) is also formed. The 1D RMSD DI is calculated according to Equation 8 using PZT SA SA_{xjk} as actuator and PZT SA as sensor. Contrary to this, PZT SA SA_{xjk} and SA'_{xjk} are used as the sensor and actuator, respectively, and DI is also calculated. Finally, the average of these two damage indices is the final index for the direction DI_{xjk} d_{xjk}. The matrix M^{yz}_{jk} is obtained by calculating 1D DI for all actuator-sensor couples in the direction parallel to x-axis LCS:

$$M^{yz}_{jk} = \begin{bmatrix} DI_{x_{11}} & DI_{x_{12}} & \dots & DI_{x_{1k}} & \dots & DI_{x_r} \\ DI_{x_{21}} & DI_{x_{22}} & \dots & DI_{x_{2k}} & \dots & DI_{x_{2r}} \\ \vdots & \vdots & \ddots & \dots & \dots & \vdots \\ DI_{x_{j1}} & DI_{x_{j2}} & \dots & DI_{x_{jk}} & \dots & DI_{x_{jr}} \\ \vdots & \vdots & \vdots & \vdots & \ddots & \vdots \\ DI_{x_{q1}} & DI_{x_{q2}} & \dots & DI_{x_{qk}} & \dots & DI_{x_{qr}} \end{bmatrix} \quad (11)$$

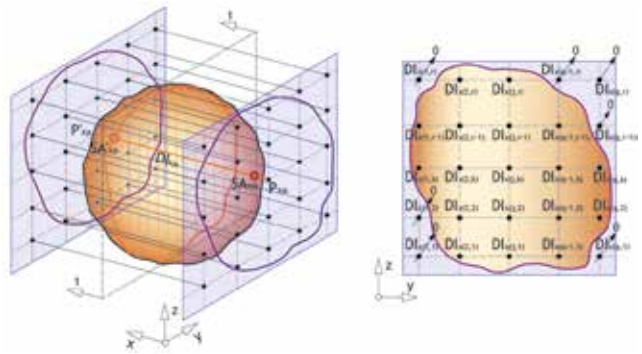

Figure 6. Procedure for forming matrix M^{yz}_{jk}

Matrix elements have zero values for all directions outside the body (Figure 6 right). In the general case, values are different from zero for the directions inside the body. Similarly, matrix M^{yz}_{jk} is formed for directions parallel to y-axis, equation (12), while matrix M^{yz}_{ij} is formed for directions parallel to z-axis, Equation (13):

$$M^{yz}_{ik} = \begin{bmatrix} DI_{y_{11}} & DI_{y_{12}} & \dots & DI_{y_{1k}} & \dots & DI_{y_{1r}} \\ DI_{y_{21}} & DI_{y_{22}} & \dots & DI_{y_{2k}} & \dots & DI_{y_{2r}} \\ \vdots & \vdots & \ddots & \vdots & \dots & \vdots \\ DI_{y_{i1}} & DI_{y_{i2}} & \dots & DI_{y_{ik}} & \dots & DI_{y_{ir}} \\ \vdots & \vdots & \vdots & \vdots & \ddots & \vdots \\ DI_{y_{p1}} & DI_{y_{p2}} & \dots & DI_{y_{pk}} & \dots & DI_{y_{pr}} \end{bmatrix} \quad (12)$$

$$M^{yz}_{ij} = \begin{bmatrix} DI_{z_{11}} & DI_{z_{12}} & \dots & DI_{z_{1j}} & \dots & DI_{z_{1q}} \\ DI_{z_{21}} & DI_{z_{22}} & \dots & DI_{z_{2j}} & \dots & DI_{z_{2q}} \\ \vdots & \vdots & \ddots & \vdots & \dots & \vdots \\ DI_{z_{i1}} & DI_{z_{i2}} & \dots & DI_{z_{ij}} & \dots & DI_{z_{iq}} \\ \vdots & \vdots & \vdots & \vdots & \ddots & \vdots \\ DI_{z_{p1}} & DI_{z_{p2}} & \dots & DI_{z_{pj}} & \dots & DI_{z_{pq}} \end{bmatrix} \quad (13)$$

Matrix M^{yz}_{ij} is pxq, matrix M^{xz}_{ik} is pxr, while matrix M^{yz}_{jk} is qxr.
Finally, a novel three-dimensional damage index SDI, represented by 3D matrix, is derived by index multiplying matrix elements (11), (12) and (13):

$$SDI_{ijk} = M^{xy}_{ij} \bar{\bullet} M^{xz}_{ik} \bar{\bullet} M^{yz}_{jk} \quad (14)$$

where SDI_{ijk} is 3D matrix pxqxr, while the operator $\bar{\bullet}$ stands for

multiplying matrix terms depending on their position in the matrix (lower index). For example, for i = 3, j = 5 and k = 7, the element of the 3D matrix SDI_{357} is obtained by multiplying the element DI_{z35} of the matrix M_{ij}^{xy} by the element DI_{z37} of the matrix M_{ik}^{xz} and the element DI_{z57} of the matrix M_{jk}^{yz}. The notation of the 3D matrix can be presented in three different ways: with respect to XY plane Equation (15) and (16), with respect to XZ plane, Equation (18), or with respect to YZ plane, Equation (19):

$$SDI_{pqr}^{xy} = \tag{15}$$

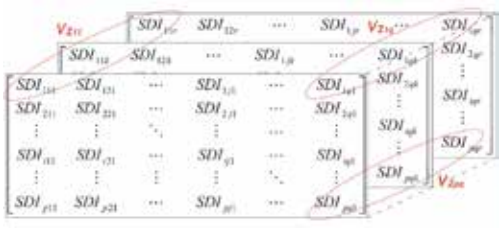

$$SDI_{pqr}^{xy} = \begin{bmatrix} \mathbf{V}_{z_{11}} & \mathbf{V}_{z_{12}} & \cdots & \mathbf{V}_{z_{1j}} & \cdots & \mathbf{V}_{z_{1q}} \\ \mathbf{V}_{z_{21}} & \mathbf{V}_{z_{22}} & \cdots & \mathbf{V}_{z_{2j}} & \cdots & \mathbf{V}_{z_{2q}} \\ \vdots & \vdots & \ddots & \vdots & \cdots & \vdots \\ \mathbf{V}_{z_{i1}} & \mathbf{V}_{z_{i2}} & \cdots & \mathbf{V}_{z_{ij}} & \cdots & \mathbf{V}_{z_{iq}} \\ \vdots & \vdots & \vdots & \vdots & \ddots & \vdots \\ \mathbf{V}_{z_{p1}} & \mathbf{V}_{z_{p2}} & \cdots & \mathbf{V}_{z_{pj}} & \cdots & \mathbf{V}_{z_{pq}} \end{bmatrix} \tag{16}$$

Labelling of 3D matrix has been adopted in a similar way as with standard 2D matrix, the only exception being that its elements are vectors. Vectors of the matrix shown in Equation (16) are of dimension r:

$$\mathbf{V}_{z_{ij}} = \left\{SDI_{ij1}, SDI_{ij2}, ..., SDI_{ijk}, ..., SDI_{ijr}\right\} \tag{17}$$

The 3D matrix in notation with respect to XZ and YZ planes is represented by equations (18) and (19) respectively:

$$SDI_{prq}^{xz} = \begin{bmatrix} \mathbf{V}_{y_{11}} & \mathbf{V}_{y_{12}} & \cdots & \mathbf{V}_{y_{1k}} & \cdots & \mathbf{V}_{y_{1r}} \\ \mathbf{V}_{y_{21}} & \mathbf{V}_{y_{22}} & \cdots & \mathbf{V}_{y_{2k}} & \cdots & \mathbf{V}_{y_{2r}} \\ \vdots & \vdots & \ddots & \vdots & \cdots & \vdots \\ \mathbf{V}_{y_{i1}} & \mathbf{V}_{y_{i2}} & \cdots & \mathbf{V}_{y_{ik}} & \cdots & \mathbf{V}_{y_{ir}} \\ \vdots & \vdots & \vdots & \vdots & \ddots & \vdots \\ \mathbf{V}_{y_{p1}} & \mathbf{V}_{y_{p2}} & \cdots & \mathbf{V}_{y_{pk}} & \cdots & \mathbf{V}_{y_{pr}} \end{bmatrix} \tag{18}$$

$$SDI_{qrp}^{yz} = \begin{bmatrix} V_{x_{11}} & V_{x_{12}} & ... & V_{x_{1k}} & ... & V_{x_{1r}} \\ V_{x_{21}} & V_{x_{22}} & ... & V_{x_{2k}} & ... & V_{x_{2r}} \\ \vdots & \vdots & \ddots & \vdots & ... & \vdots \\ V_{x_{j1}} & V_{x_{j2}} & ... & V_{x_{jk}} & ... & V_{x_{jr}} \\ \vdots & \vdots & \vdots & \vdots & \ddots & \vdots \\ V_{x_{q1}} & V_{x_{q2}} & ... & V_{x_{qk}} & ... & V_{x_{qr}} \end{bmatrix} \tag{19}$$

Regardless of the way in which the 3D matrix is presented, the values of its elements for each sub-domain have unique values. The total damage index U_o is defined in the following way:

$$U_o = \sum_{i=1}^{p}\sum_{j=1}^{q}\sum_{k=1}^{r}\beta_{ijk}\cdot SDI_{ijk} \tag{20}$$

where β_{ijk} are the weighting coefficients determined based on the participation of the respective sub-domain in the total volume:

$$\beta_{ijk} = \frac{V_{ijk}}{\sum_{i=1}^{p}\sum_{j=1}^{q}\sum_{k=1}^{r}V_{ijk}} \tag{21}$$

with the following notation: V_{ijk} - volume of the sub-domain B_{ijk} represented by the point T_{ijk}. With SDI_{ijk}, we obtain the information about damage inside the RC element for separate sub-domains, while the total damage index U_o defines an overall element damage. The higher value of damage index indicates higher damage inside a RC element.

5. Numerical simulation

Numerical modelling of PZT SA and wave propagation was performed according to the finite element method using the commercial software ABAQUS 6.11. PZT SA models were analysed using the quasi-static analysis with the standard FEM, while the wave propagation models were constructed using the explicit FEM. The applied modelling method using the standard FEM and a quasi-static analysis of the PZT SA and the explicit FEM for modelling ultrasonic wave propagation, was successfully used on several occasions [31, 32]. It was presented for the first time in the research in which the numerical approach was experimentally verified on concrete beams with and without damagea [33].

5.1. FE modelling of PZT SA

Piezoelectric patches can produce two different effects: sensor effect, and actuator effect. This ability of PZT patches allows them to be used as actuators and as sensors, which can significantly reduce the required number of PZT SA in RC structures monitoring operations.

The FE modelling of piezoelectric materials is based on constitutive equations for coupled electro-mechanical behaviour. The coupled electro-mechanical behaviour of piezoelectric materials is defined with Eqs. (22) and (23):

$$\sigma_{ij} = D_{ijkl}^{E}\left(\varepsilon_{kl} - d_{mkl}^{\varphi}E_m\right) \tag{22}$$

$$q_i = e_{ijk}^{\varphi}\varepsilon_{jk} + D_{ij}^{\varphi(\varepsilon)}E_j \tag{23}$$

with the following notation:

σ_{ij}, ε_{ij} - mechanical stress and strain tensor

q_i - electric "displacement" vector
D^E_{ijkl} - material's elastic stiffness matrix defined at zero electrical potential gradient
d^{φ}_{mkl} - material's piezoelectric strain coefficient matrices
E_i - electrical potential gradient vector;
$D^{\varphi(\varepsilon)}_{ij}$ - material's dielectric properties strain matrix.

The piezoelectric effect is governed by coupled mechanical equilibrium and electric flux conservation equations [34]. The mechanical equilibrium is defined by Equation (24) and electrical flux conservation is defined by Equation (25):

$$\int_V \sigma : \delta\varepsilon dV = \int_S t \cdot \delta u dS + \int_V f \cdot \delta u dV \tag{24}$$

$$\int_V q : \delta E dV = \int_S q_S \cdot \delta\varphi dS + \int_V q_V \cdot \delta\varphi dV \tag{25}$$

where:
σ - the Cauchy stress
t - the traction across a point on the surface of the body
f - the body force per unit volume
q - the electric flux
q_S - the electric flux per unit area entering the body at a point on its surface
q_V - the electric flux entering the body per unit volume.

Electric potentials and displacement for the piezoelectric elements exist at nodal locations, and they are approximated with interpolation functions.

Young's modulus	Poisson's ratio	Mass density
30 GPa	0.1	2400 kg/m³
Rayleigh damping	$\alpha = 0.01$	$\beta = 5 \cdot 10^{-8}$

Table 1. Material properties of concrete

Material properties of the piezoelectric patch used in this study are presented by equations (26), (27) and Table 2. The orthotropic model was used for dielectric and piezoelectric properties of PZT material (Equation 26). Mechanical properties are described by the use of orthotropic elasticity, by specifying the terms in the elastic stiffness matrix (Equation 27). Concrete block is modelled as the linearly elastic material having the properties as shown in Table 1. The contact between the PZT plate and the surrounding concrete is defined using the surface-based tie constraints, simulating a complete connection between these two parts. The applied constraint (Tie Constraint) ties two separate surfaces together so that there is no relative motion between them.

$$\left[D^{\varphi(\varepsilon)}_{ij}\right] = \begin{bmatrix} D^{\varphi(\varepsilon)}_{11} & 0 & 0 \\ 0 & D^{\varphi(\varepsilon)}_{22} & 0 \\ 0 & 0 & D^{\varphi(\varepsilon)}_{33} \end{bmatrix} \tag{26}$$

$$\left[d^{\varphi}_{mkl}\right] = \begin{bmatrix} 0 & 0 & 0 & 0 & d^{\varphi}_{113} & 0 \\ 0 & 0 & 0 & d^{\varphi}_{212} & 0 & 0 \\ d^{\varphi}_{311} & d^{\varphi}_{322} & d^{\varphi}_{333} & 0 & 0 & 0 \end{bmatrix}$$

$$\left[D^{e}_{ijkl}\right] = \begin{bmatrix} D_{1111} & D_{1122} & D_{1133} & 0 & 0 & 0 \\ D_{1122} & D_{2222} & D_{2233} & 0 & 0 & 0 \\ D_{1133} & D_{2233} & D_{3333} & 0 & 0 & 0 \\ 0 & 0 & 0 & D_{1212} & 0 & 0 \\ 0 & 0 & 0 & 0 & D_{1313} & 0 \\ 0 & 0 & 0 & 0 & 0 & D_{2323} \end{bmatrix} \tag{27}$$

where:
$D^{\varphi(\varepsilon)}_{ij}$ - dielectric matrix
d^{φ}_{mkl} - piezoelectric strain matrix
D^{e}_{ijkl} - stiffness matrix.

The quasi-static analysis was performed by applying a constant electrical voltage (from 0V to 100V with 10V step),

Table 2. Material properties of piezoelectric patch

Dielectric properties [F/m]		
$D^{\varphi(\varepsilon)}_{11} = 1.46 \cdot 10^{-8}$	$D^{\varphi(\varepsilon)}_{22} = 1.46 \cdot 10^{-8}$	$D^{\varphi(\varepsilon)}_{33} = 1.55 \cdot 10^{-8}$
Piezoelectric properties [C/m²]		
$d^{\varphi}_{311} = d^{\varphi}_{322} = -1.74 \cdot 10^{-8}$	$d^{\varphi}_{333} = 3.94 \cdot 10^{-8}$	$d^{\varphi}_{212} = d^{\varphi}_{113} = 5.35 \cdot 10^{-8}$
Mechanical properties [N/m²]		
$D_{1111} = D_{2222} = 12.29 \cdot 10^{-10}$	$D_{1122} = 7.66 \cdot 10^{-10}$	$D_{1133} = D_{2233} = 7.02 \cdot 10^{-10}$
$D_{3333} = 9.71 \cdot 10^{-10}$	$D_{1212} = 2.32 \cdot 10^{-10}$	$D_{1313} = D_{2323} = 2.23 \cdot 10^{-10}$

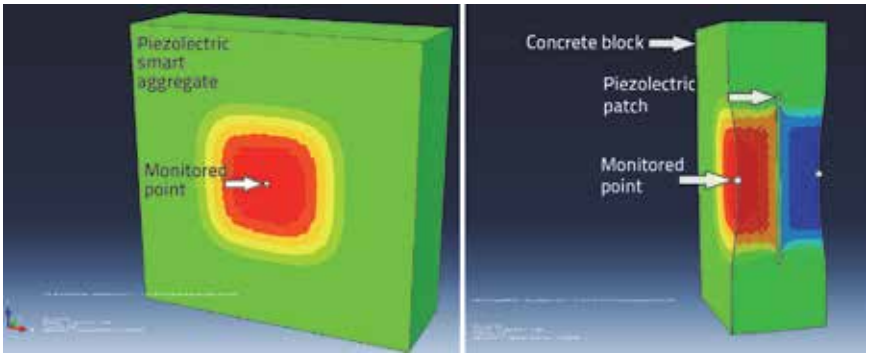

Figure 7. Displacement U_2 of PZT SA: Entire model (left); Cross-section through main central vertical plane (right)

and deformation of the concrete block was monitored at a predetermined point (see Figure 7). The obtained results reveal a linear relationship between the applied electric voltage and the displacement at a monitored point. On the basis of the obtained linear relationship, the displacement obtained in the SA model is used for wave propagation modelling.

5.2. FE modelling of wave propagation with EFEM

The ultrasound wave propagation is analysed according to the explicit FEM using the commercial software ABAQUS /EXPLICIT. The program utilizes an explicit scheme of the Newmark integration method based on the central difference for the solution of the governing system of equations of motion. The time range [0, T] is adopted and equally divided into Nsub-domains $[t_n, t_{n+1}]$, where $0 = t_0 < t_1 < \ldots < t_n = T$, $t_{n+1} - t_n = \Delta t = T/N$. Displacements, velocities and accelerations, approximated with the central-difference scheme (Equation 28), are represented using truncated Taylor's series:

$$\begin{cases} \partial_t u^h_{n+1/2} = \left(u^h_{n+1} - u^h_n\right) / \Delta t \approx \dot{u}^h_{n+1/2} \\ \partial_{t^2} u^h_n = \left(u^h_{n+1} - 2u^h_n + u^h_{n-1}\right) / \Delta t^2 \\ \ddot{u}^h_n \approx \left(\dot{u}^h_{n+1/2} - \dot{u}^h_{n-1/2}\right) / \Delta t \end{cases} \tag{28}$$

The stability of solutions depends on the speed of propagation of longitudinal waves and on the smallest characteristic dimension of the finite element:

$$\Delta t \le \Delta t_{crit} = \frac{\Delta L}{c_L} \tag{29}$$

where:

ΔL - smallest characteristic dimension of the finite element
Δt - time increment
Δt_{crit} - critical time increment
cL - velocity of longitudinal wave

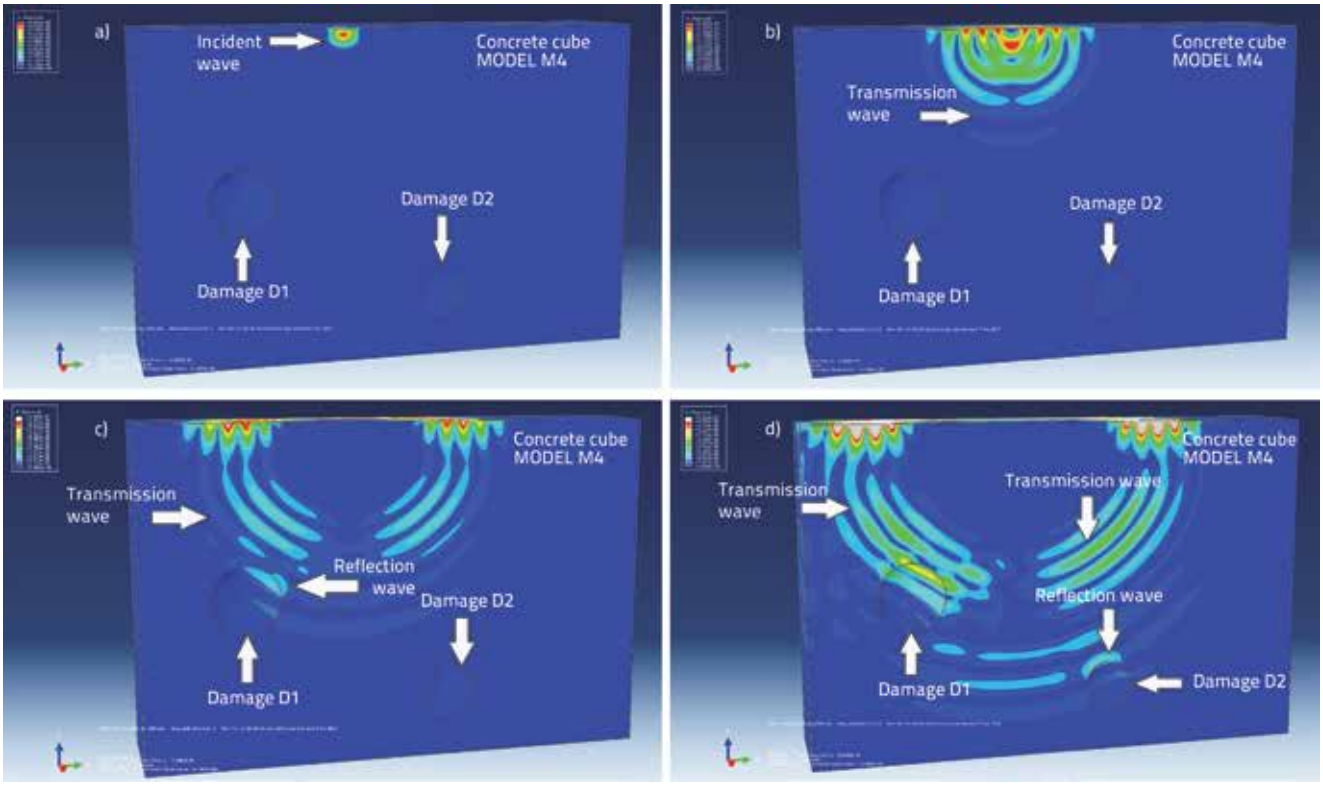

Figure 8. Wave field for Model M4 generated by the PZT SA actuator at various time instances: a) $t = 2.50 \cdot 10^{-5}$s; b) $t = 5.00 \cdot 10^{-5}$s; c) $t = 7.50 \cdot 10^{-5}$s; d) $t = 8.00 \cdot 10^{-5}$s

From Equation (29) it follows that it is necessary to use less time step for smaller dimensions of finite elements. Causally, characteristic values are calculated for the entire model for each time step, so that the computation cost increases for a smaller Δt. Also, it is necessary to apply at least seven finite elements per wavelength for the wave propagation modelling. Therefore, relatively small models require very powerful computers. It follows that it is necessary to select an optimum model from the point of view of the reliability of results and calculation complexity. It is absolutely impossible to perform numerical analysis on models of real size elements of RC structures.

Displacement results based on the PZT SA models were applied for modelling actuators using the ABAQUS/EXPLICIT software. The displacement normal to the PZT plate surface, defined using the boundary conditions, was imposed as a function of the input signal (3.5-cycle Hanning-windowed tone burst) with the central frequency of 100 kHz. The sensor output signals were derived by measuring displacements normal to the PZT patch surface of the SA sensor. The finite element size of 2.0 mm was adopted (12 FEs per wavelength). The C3D8R element was adopted: an 8-node linear brick element, with reduced integration, and hourglass control.

6. Numerical examples

The proposed 3D DI was verified numerically by analysing different cases, which included varying geometry of a model, the position and size of damage, number of occurrences of damage, number of planes of intersections, and number of PZT SA. Analysed numerical models are shown in Figures 9 and 10. First two models have three intersection planes in all three orthogonal directions. Model M1 has symmetric damage while damage is asymmetric in model M2. The diameter of the damage is 4cm in both cases. In models M3 and M4 the number of intersections in x and z directions is 3, while in y it is 4. In the third model, damage is 4cm in diameter, while the fourth model has 2 damage diameters (4cm and 3cm) which are positioned asymmetrically. The ball shape of damage was considered. Relatively small dimensions of numerical models were chosen because of computational demands, taking into account the applied frequency and velocity of longitudinal waves. Applied models required around one million finite elements. The size of damage, considering that it was an artificially generated hole in concrete element, was adopted to be higher than wavelength used in simulation.

Appropriate models were constructed in ABAQUS/EXPLICIT for all four analysed scenarios, and wave propagation simulations were conducted for all possible PZT SA sensor/actuator combinations. For all sensors, output signals were read in time domain for an intact model and damage models. An original program was written in MATLAB software according to the procedure shown in sections 3 and 4:

- the energy of all decomposed signals obtained from wavelet signal decomposition of output sensor signals was calculated
- linear RMSD damage indices for all actuator-sensor couples were calculated according to obtained energies
- matrices of damage index were formed for three orthogonal directions (M_{jk}^{yz}, M_{ij}^{xy} and M_{ik}^{xz})
- 3D matrices were calculated according to Eqs. (16, 18 and 19)
- the total damage index was calculated according to Equation (20).

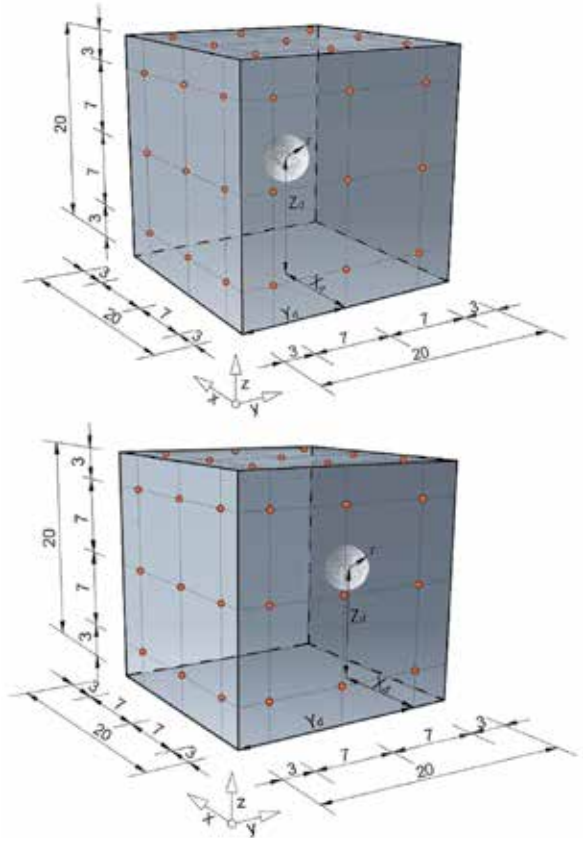

Table 3. Geometric characteristics of damage in applied models

	Model M1	Model M2	Model M3	Model M4	
Damage characteristics	r = 2 cm	r = 2 cm	r = 2 cm	r = 2 cm	r = 1.5 cm
	X_d = 10 cm	X_d = 17 cm	X_d = 7 cm	X_{d1} = 7 cm	X_{d2} = 7 cm
	Y_d = 10 cm	Y_d = 10 cm	Y_d = 12 cm	Y_{d1} = 6 cm	Y_{d2} = 18 cm
	Z_d = 10 cm	Z_d = 10 cm	Z_d = 10 cm	Z_{d1} = 10 cm	Z_{d2} = 4 cm

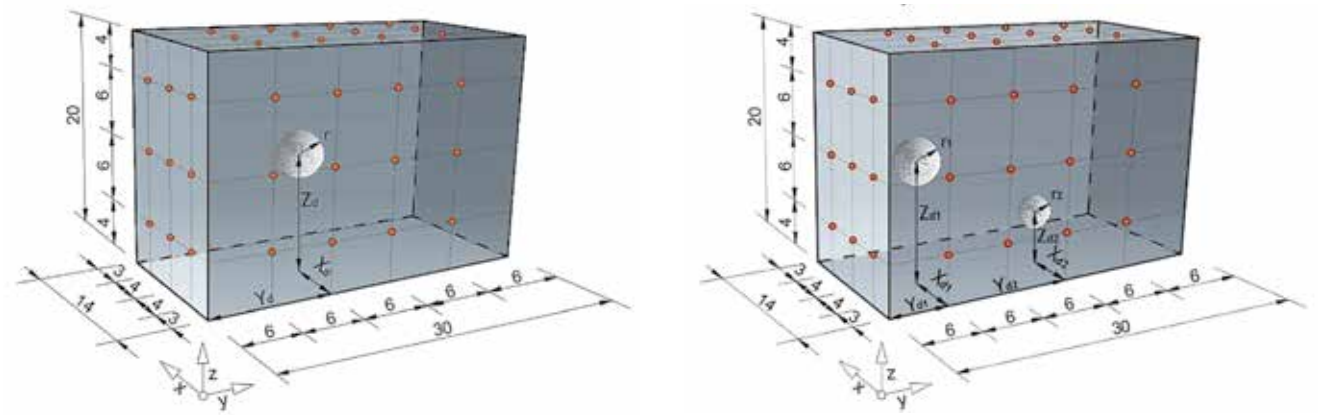

Figure 10. Geometry of models and position of PZT SA: Model M3 (left); Model M4 (right), (lengths in cm)

Figure 9. Geometry of models and position of PZT SA: Model M1 (top); Model M2 (bottom), (lengths in cm)

7. Results and discussion

3D damage indices and the total DI for the analysed numerical scenarios are presented in Figures 11 and 12 and in Table 4. The 3D DI for model M1 with the central damage position is shown in Figure 11 left. The results are illustrated by the graph showing the matrix created according to xy planes. It can clearly be seen in Figure 11 left (middle graph) that the value of DI at

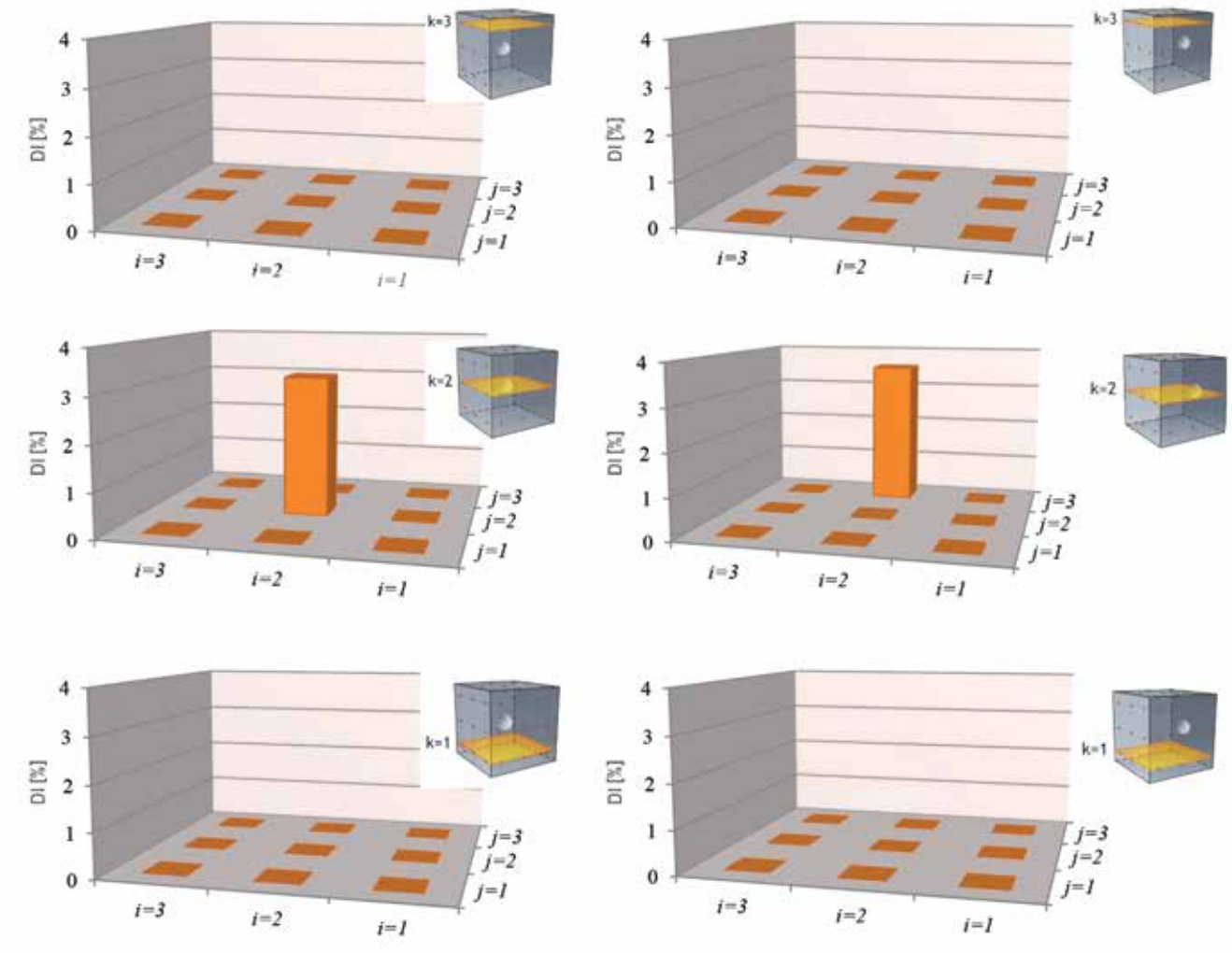

Figure 11. Results of three-dimensional damage indices: Model M1 (left); Model M2 (right)

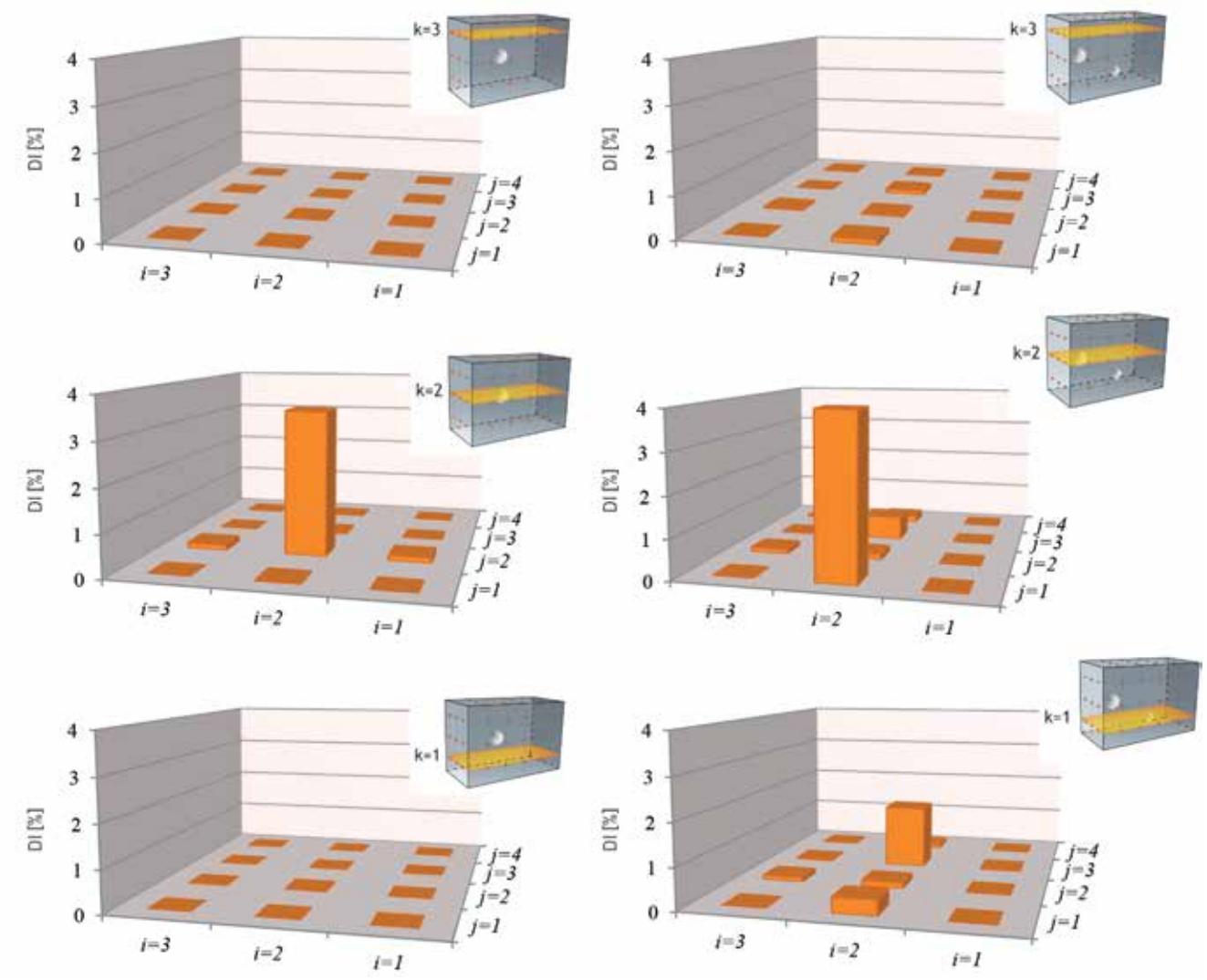

Figure 12. Results of three-dimensional damage indices: : Model M3 (left); Model M4 (right)

sub-domain B_{222} is the highest, which completely correlates with the position of the given damage. Further, damage index values for the rest of sub-domains are different from zero but are very small in relation to DI for sub-domain where the damage is actually situated.

Similarly to model M1, the results for model M2 are presented in Figure 11 right. It can be seen that the value of damage index is the highest for sub-domain B_{232} and that it correlates with the position of damage. The results of 3D DI and total DI for models M1 and M2 are shown in Table 1. A more detailed analysis of results shows that values of the component 3D DI at the position of damage for model M1 and M2 slightly differ. The results of models M3 and M4 are presented in Figure 12 left and right. For model M3, the positions of damage and of the highest component of 3D DI coincide completely. This position is in sub-domain B_{222}. It can be observed that sub-domains B_{122} and B_{322} have a slightly bigger value than other components of 3D DI without damage, but this value is still very small in relation to the value of the component where damage is located. Two significant values of DI can be seen in model M4 that has two instances of damage. These values correspond to the position of damage (sub-domains B_{212} and B_{231}). For all models, the largest member of the 3D matrix completely coincides with the position of damage, which shows that the damage index can localize damage in the volume of a sub-domain. Considering that instances of damage differ in size (one 4cm the other 3cm), it can be seen in Table 3 and in Figure 12 right that the component of 3D DI for sub-domain, where the damage is bigger, is considerably bigger than the value where the damage is smaller. According to this model, we can conclude that the suggested damage index is sensitive to the size of damage. Comparing the values of the total damage index for models M3 and M4, which are geometrically identical and have the same number of PZT SA, but model M4 is more damaged, it can be noticed that the total damage index for M4 is bigger than the value for M3. This shows that the proposed total damage index

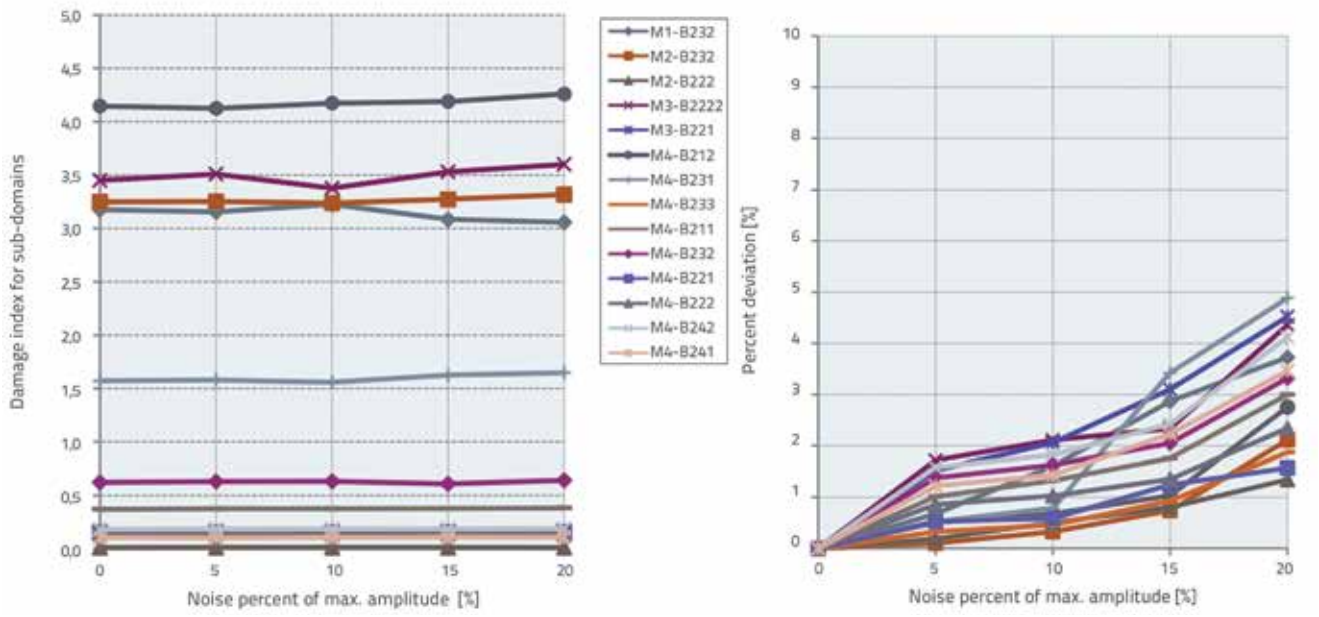

Figure 13. Relation of DI change depending on the level of implemented noise (left); Percent deviation of DI changes depending on the level of implemented noise (right)

Table 4. Values of 3D DI vectors and total damage indices

MODEL 1		**MODEL 2**	
Matrix form	Vector values [%]	Matrix form	Vector values [%]
$\begin{bmatrix} V_{z_{11}} & V_{z_{12}} & V_{z_{13}} \\ V_{z_{21}} & V_{z_{22}} & V_{z_{23}} \\ V_{z_{31}} & V_{z_{32}} & V_{z_{33}} \end{bmatrix}$	$Vz_{11}=\{0.022\cdot10^{-4}; 0.212\cdot10^{-4}; 0.022\cdot10^{-4}\}$	$\begin{bmatrix} V_{z_{11}} & V_{z_{12}} & V_{z_{13}} \\ V_{z_{21}} & V_{z_{22}} & V_{z_{23}} \\ V_{z_{31}} & V_{z_{32}} & V_{z_{33}} \end{bmatrix}$	$Vz_{11}=\{0.025\cdot10^{-4}; 0.036\cdot10^{-4}; 0.025\cdot10^{-4}\}$
	$Vz_{12}=\{0.212\cdot10^{-4}; 0.239\cdot10^{-2}; 0.212\cdot10^{-4}\}$		$Vz_{12}=\{0.0931\cdot10^{-4}; 0.232\cdot10^{-4}; 0.0931\cdot10^{-4}\}$
	$Vz_{13}=\{0.022\cdot10^{-4}; 0.212\cdot10^{-4}; 0.022\cdot10^{-4}\}$		$Vz_{13}=\{0.743\cdot10^{-4}; 0.328\cdot10^{-2}; 0.743\cdot10^{-4}\}$
	$Vz_{21}=\{0.212\cdot10^{-4}; 0.239\cdot10^{-2}; 0.212\cdot10^{-4}\}$		$Vz_{21}=\{0.036\cdot10^{-4}; 0.013\cdot10^{-2}; 0.036\cdot10^{-4}\}$
	$Vz_{22}=\{0.239\cdot10^{-2}; \mathbf{3.176}; 0.239\cdot10^{-2}\}$		$Vz_{22}=\{0.336\cdot10^{-4}; 0.0109; 0.336\cdot10^{-4}\}$
	$Vz_{23}=\{0.212\cdot10^{-4}; 0.239\cdot10^{-2}; 0.212\cdot10^{-4}\}$		$Vz_{23}=\{0.328\cdot10^{-2}; \mathbf{3.250}; 0.328\cdot10^{-2}\}$
	$Vz_{31}=\{0.022\cdot10^{-4}; 0.212\cdot10^{-4}; 0.022\cdot10^{-4}\}$		$Vz_{31}=\{0.025\cdot10^{-4}; 0.036\cdot10^{-4}; 0.025\cdot10^{-4}\}$
	$Vz_{32}=\{0.212\cdot10^{-4}; 0.239\cdot10^{-2}; 0.212\cdot10^{-4}\}$		$Vz_{32}=\{0.0931\cdot10^{-4}; 0.232\cdot10^{-4}; 0.0931\cdot10^{-4}\}$
	$Vz_{33}=\{0.022\cdot10^{-4}; 0.212\cdot10^{-4}; 0.022\cdot10^{-4}\}$		$Vz_{33}=\{0.743\cdot10^{-4}; 0.328\cdot10^{-2}; 0.743\cdot10^{-4}\}$
Total damage index: $\mathbf{U_0 = 0.141}$ [%]		Total damage index: $\mathbf{U_0 = 0.148}$ **[%]**	
MODEL 3		**MODEL 4**	
Matrix form	Vector values [%]	Matrix form	Vector values [%]
$\begin{bmatrix} V_{z_{11}} & V_{z_{12}} & V_{z_{13}} & V_{z_{14}} \\ V_{z_{21}} & V_{z_{22}} & V_{z_{23}} & V_{z_{24}} \\ V_{z_{31}} & V_{z_{32}} & V_{z_{33}} & V_{z_{34}} \end{bmatrix}$	$Vz_{11}=\{0.22\cdot10^{-4}; 0.48\cdot10^{-2}; 0.22\cdot10^{-4}\}$	$\begin{bmatrix} V_{z_{11}} & V_{z_{12}} & V_{z_{13}} & V_{z_{14}} \\ V_{z_{21}} & V_{z_{22}} & V_{z_{23}} & V_{z_{24}} \\ V_{z_{31}} & V_{z_{32}} & V_{z_{33}} & V_{z_{34}} \end{bmatrix}$	$Vz_{11}=\{0.011; 0.024; 0.542\cdot10^{-4}\}$
	$Vz_{12}=\{0.18\cdot10^{-3}; 0.1407; 0.18\cdot10^{-3}\}$		$Vz_{12}=\{0.024; 0.024; 0.608\cdot10^{-3}\}$
	$Vz_{13}=\{0.22\cdot10^{-4}; 0.54\cdot10^{-3}; 0.22\cdot10^{-4}\}$		$Vz_{13}=\{0.041; 0.022; 0.291\cdot10^{-3}\}$
	$Vz_{14}=\{0.12\cdot10^{-5}; 0.31\cdot10^{-4}; 0.12\cdot10^{-5}\}$		$Vz_{14}=\{0.016; 0.029; 0.027\}$
	$Vz_{21}=\{0.83\cdot10^{-3}; 0.37\cdot10^{-2}; 0.83\cdot10^{-3}\}$		$Vz_{21}=\{0.371; \mathbf{4.146}; 0.127\}$
	$Vz_{22}=\{0.0245; \mathbf{3.451}; 0.0245\}$		$Vz_{22}=\{0.152; 0.150; 0.052\}$
	$Vz_{23}=\{0.83\cdot10^{-3}; 0.37\cdot10^{-2}; 0.83\cdot10^{-3}\}$		$Vz_{23}=\{\mathbf{1.572}; 0.622; 0.112\}$
	$Vz_{24}=\{0.31\cdot10^{-4}; 0.14\cdot10^{-3}; 0.31\cdot10^{-4}\}$		$Vz_{24}=\{0.104; 0.181; 0.032\}$
	$Vz_{31}=\{0.22\cdot10^{-4}; 0.48\cdot10^{-2}; 0.22\cdot10^{-4}\}$		$Vz_{31}=\{0.011; 0.024; 0.542\cdot10^{-4}\}$
	$Vz_{32}=\{0.18\cdot10^{-3}; 0.1407; 0.18\cdot10^{-3}\}$		$Vz_{32}=\{0.123; 0.122; 0.042\}$
	$Vz_{33}=\{0.22\cdot10^{-4}; 0.54\cdot10^{-3}; 0.22\cdot10^{-4}\}$		$Vz_{33}=\{0.041; 0.022; 0.291\cdot10^{-3}\}$
	$Vz_{34}=\{0.12\cdot10^{-5}; 0.31\cdot10^{-4}; 0.12\cdot10^{-5}\}$		$Vz_{34}=\{0.016; 0.029; 0.027\}$
Total damage index: $\mathbf{U_0 = 0.154}$ [%]		Total damage index: $\mathbf{U_0 = 0.293}$ **[%]**	

is sensitive to the appearance of new instances of damage and that it can be used for monitoring RC structures.

The results obtained by numerical simulations of various possible cases of damage in concrete models show that the proposed approach of damage detection by 3D DI is promising. In future research, It will be necessary to experimentally verify the suggested approach on both small models and real-size RC elements. For practical application of the proposed 3D DI in damage detection and SHM, it would be necessary to do experimental measurements on real structures.

The sensitivity analysis was conducted to determine the change of damage index according to the implemented level of noise. This analysis was performed in order to see practical potential of the proposed 3D DI. The analysis of damage index for sub-domains change depending on the level of implemented noise is presented in Figure 13. The maximum amplitude of the Gaussian white noise was adopted as percentage values (5%, 10%, 15% and 20%) of the maximum amplitude for the intact model. Afterwards, it was applied to the intact and damaged models, so that both considered cases incorporated the same level of noise. From the accompanying results (Figure 13), it is obvious that the damage index is almost insensitive to noise change. Even in the case of 20% of the max amplitude, the change of the damage index is marginal only (smaller than 5%).

8. Conclusions

A novel approach of active monitoring and non-destructive damage detection in concrete structures, based on the PZT SA, is presented. A novel three-dimensional damage index was developed in matrix form according to the wavelet signal decomposition and energy of wave propagation. The present approach demands the application of PZT SA embedded or set on the surface of a concrete element. The novel 3D DI was derived for an arbitrary shape of a concrete element and for a number of orthogonal intersection planes. The verification was conducted numerically by applying the standard FEM for PZT SA modelling and explicit FEM for wave propagation modelling. Output signals at sensor positions were decomposed by wavelet signal decomposition and 1D RMSD damage index was calculated. This damage index was used as the input parameter for forming a 3D DI. The three-dimensional DI was calculated for four distinct numerical scenarios in which positions and sizes were varied, as well as the geometry of the model and the number of PZT SA used. For all analysed damage positions in models, the biggest components of 3D DI were at the place of sub-domain where damage was situated. The total damage index was obtained for all analysed models, and it was established that the value is bigger for more damaged models as compared to less damaged models.

The approach of non-destructive damage detection in space can be used for standard RC structures, but it is more suited for massive concrete elements of civil-engineering structures. In this respect, the approach calls for the use of a relatively big number of PZT SA. It is recommended to apply them to the parts that are of special significance for structural capacity and stability as well as for the parts that are unavailable for visual inspection. The proposed novel damage index can also be applied for monitoring the existing structures with concrete elements in historic masonry buildings.

For all analysed numerical models, the largest member of the 3D matrix completely coincides with the position of damage, which shows that the damage index can localize damage in the volume of a sub-domain. Based on the results obtained in this research, it can be deduced that damage index is only slight sensitive to noise change. Even in the case of noise amplitude of 20% of the max signal amplitude for intact model, the change of the damage index is smaller than 5%. The applied approach of 3D damage detection is characterized by very good features which are also related to PZT SA use. These features are: a) wide frequency range, b) quick response, c) low price, d) possibility of active monitoring of damage in time, e) possibility of using the same PZT SA as both the actuator and sensor, and f) possibility of detecting damage locally inside a massive RC element. Finally, based on the results obtained during analysis of various models, it can be concluded that the proposed 3D damage index is potentially quite promising. Further research will certainly involve experimental verification of the suggested approach.

Acknowledgments

This research was supported by SEEFORM (South Eastern graduate school for Master and PhD Formation in Engineering) and DAAD (Deutscher Akademischer Austauschdients – German Academic Exchange Service).

REFERENCES

[1] Hu, B., Kundu, T., Grill, W., Liu, B., Toufigh, V.: Embedded piezoelectric sensors for health monitoring of concrete structures, American Concrete Institute (ACI) Materials Journal, 110 (2013) 2, pp. 149-158

[2] Lu, Y., Li, J., Ye, L., Wang D.: Guided waves for damage detection in rebar-reinforced concrete beams, Construction and Building Materials, 47 (2013), pp. 370-378

[3] Liao, W.I., Wang, J.X., Song, G., Gu, H., Olmi, C., Mo, Y.L., Chang, K.C., Loh, C.H.: Structural health monitoring of concrete columns subjected to seismic excitations using piezoceramic-based sensors, Smart Materials and Structures, 20 (2011), pp. 10

[4] Howser, R., Moslehy, Y., Gu, H., Dhonde, H., Mo, Y.L., Ayoub, A., Song, G.: Smart-aggregate-based damage detection of fibre-reinforced-polymer-strengthened columns under reverse cyclic loading, Smart Materials and Structures, 20 (2011), pp. 9

[5] Laskar, A., Gu, H., Mo, Y.L., Song, G.: Progressive collapse of a two-story reinforced concrete frame with embedded smart aggregates, Smart Materials and Structures, 18 (2009), pp. 10

[6] Dong, B. et al: In-situ structural health monitoring of a reinforced concrete frame embedded with cement-based piezoelectric smart composites, Research in nondestructive evaluation, 27 (2016) 4

[7] Betz, D.C., Staszewski, W.J., Thursby, G., Culshaw, B.: Structural damage identification using multifunctional Bragg grating sensors: II.: Damage detection results and analysis, Smart Materials and Structures, 15 (2006), pp. 1313-1322

[8] Rizzo, P., Scalea, F.L.: Feature extraction for damage detection in strands by guided ultrasonic waves, Structural Health Monitoring, 5 (2006) 3, pp. 297-308

[9] Park S., Yun, C.B., Roh, Y., Lee, J.J.: PZT-based active damage detection techniques for steel bridge components, Smart Materials and Structures, 15 (2006), pp. 957-966

[10] Stojić, D., Nestorović, T., Marković, N., Cvetković, R., Stojić, N.: Detection of damage to reinforced-concrete structures using piezoelectric smart aggregates, Građevinar, 68 (2016) 5, pp. 371-380, doi: https://doi.org/10.14256/JCE.1372.2015

[11] Qing, X.P., Chan, H.L., Beard, S.J., Kumar, A.: An active diagnostic system for structural health monitoring of rocket engines, Journal of Intelligent Materials Systems and Structures, 17 (2006) 7, pp. 619-628

[12] Wu, Z., Qing, X.P., Ghosh, K., Karbhar, V., Chang, F.K.: Health monitoring of bonded composite repair in bridge rehabilitation, Smart Materials and Structures, 17 (2008), pp. 9

[13] Michaels, J.E., Michaels, T.E.: An integrated strategy for detection and imaging of damage using a spatially distributed array of piezoelectric sensors, Proceedings of the SPIE (Conference on Health Monitoring of Structures and Biological Systems), 6532 (2007), Paper No.: 653203

[14] Yuan, S., Liang, D., Shi, L., Zhao, X., Wu, Jian Li, G., Qiu, L.: Recent progress on distributed structural health monitoring research at NUAA, Journal of Intelligent Materials Systems and Structures, 19 (2008) 3, pp. 373-386

[15] Pierce, S.G., Culshaw, B., Manson, G., Worden, K., Staszewski, W.J.: The application of ultrasonic Lamb wave techniques to the evaluation of advanced composite structures, Proceedings of SPIE, (2000), Paper No. 3986, pp. 93-103

[16] Park, H.W., Sohn, H., Law, K.H., Farrar, C.R.: Time reversal active sensing for health monitoring of a composite plate, Journal of Sound and Vibration, 302 (2007), pp. 50-66

[17] Trendafilova, I., Manoach, E.: Vibration-based damage detection in plates by using time series analysis, Mechanics Systems and Signal Processing, 22 (2008), pp. 1092-1106

[18] Gao, H., Shi, Y., Rose, J.L.: Guided wave tomography on an aircraft wing with leave in place sensors, Review of Progress in Quantitative Nondestructive Evaluation 24, American Institute of Physics, Melville, New York, 2005., pp. 1788-1794

[19] Song, G., Gu, H., Mo, Y.L.: Smart aggregates: multi-functional sensors for concrete structures – a tutorial and review, Smart Materials and Structures, 17 (2008), pp. 17

[20] Shahdin, A., Morlier, J., Gourinat, Y.: Correlating low-energy impact damage with changes in modal parameteres: A preliminary study on composite beams, Structural Health Monitoring, 8 (2009) 6, pp. 523-536

[21] Cheraghi, N., Taheri, F.: A damage index for structural health monitoring based on the empirical mode decomposition, Journal of Mechanics of Materials and Structures, 2 (2007) 1, pp. 43-61

[22] Yan, S., Sun, W., Song, G., Gu, H., Huo, L.S., Liu, B., Zhang, Y.G.: Health monitoring of reinforced concrete shear walls using smart aggregates, Smart Materials and Structures, 18 (2009), pp. 6

[23] Ahmadi, H.R., Daneshjoo, F., Khaji, N.: New damage indices and algorithm based on square time-frequency distribution for damage in concrete piers of railroad bridges, Structural Control and Health Monitoring, 22 (2015), pp. 91-106

[24] Jeong, S.H., Elnashai, A.S.: New Three-Dimensional Damage Index for RC Buildings with Planar Irregularities, Journal of Structural Engineering, 9 (2006), pp. 1482-1490

[25] Kokot, S., Zembaty, Z.: Damage reconstruction of 3D frames using generic algorithms with Levenberg – Marquardt local search, Soil Dynamics and Earthquake Engineering, 29 (2009), pp. 311-323

[26] Giurgiutiu, V.: Structural health monitoring with piezoelectric wafer active sensors, Academic Press, Elsevier, San Diego, USA, 2008., pp 1-39

[27] Dumoulin, C., Karaiskos, G., Deraemaeker A.: Monitoring of crack propagation in reinforced concrete beams using embedded piezoelectric transducers, VIII International Conference on Fracture Mechanics of Concrete and Concrete Structures FraMCoS-8, Toledo, Spain, 2013.

[28] Liao, W.I., Wang, J.X., Song, G., Gu, H., Olmi, C., Mo, Y.L., Chang, K.C., Loh, C.H.: Structural health monitoring of concrete columns subjected to seismic excitations using piezoelectric-based sensors, Smart Materials and Structures, 20 (2011), pp. 10

[29] Liu, T., Zou, D., Du, C., Wang, Y.: Influence of axial loads on the health monitoring of concrete structures using embedded piezoelectric transducers, Structural Health Monitoring, 2016., pp.1-13

[30] Yan, S., Sun, W., Song, G., Gu, H., Huo, L.S., Liu, B., Zhang, Y.G.: Health monitoring of reinforced concrete shear walls using smart aggregates, Smart Materials and Structures, 18 (2009), pp. 6

[31] Marković, N., Nestorović, T., Stojić, D., Marjanović, M., Stojković, N.: Hybrid approach for two dimenzional damage localization using piezoelectric smart aggregates, Mechanics Research Communications, 85 (2017), pp. 69-75

[32] Stojić, D., Nestorović, T., Marković, N., Marjanović, M.: Experimental and numerical research on damage localization in plate-like concrete structures using hybrid approach, Structural Control and Health Monitoring, 2018., doi: https://doi.org/10.1002/stc.2214

[33] Marković, N., Nestorović, T., Stojić D.: Numerical modelling of damage detection in concrete beams using piezoelectric patches, Mechanics Research Communications, 64 (2015), pp. 15-22

[34] ABAQUS: Analysis user's manual online documentation (Version 6.11), Dassault Systems Simulia Corp., Providence, RI, USA, 2011